

Optical discrimination between spatial decoherence and thermalization of a massive object

C. Henkel¹, M. Nest², P. Domokos³, and R. Folman⁴

¹carsten.henkel@quantum.physik.uni-potsdam.de, Institut für Physik,

Universität Potsdam, D-14469 Potsdam, Germany

Universität Potsdam, Institut für Chemie, Karl-Liebknecht-Str. 25, D-14476 Potsdam, Germany

Research Institute for Solid State Physics and Optics, Budapest, Hungary

Department of Physics and Ilse Katz Center for Meso- and Nanoscale Science and Technology,

Ben Gurion University of the Negev, P.O. Box 653, Beer Sheva 84105, Israel

(Dated: 24 March 2004)

We propose a new way to observe environment-induced spatial decoherence of massive objects. The method is designed to work with a wide variety of masses, ranging from the atomic scale to nano-fabricated structures. It is based on the fact that spatial decoherence can lead to the build-up of coherences between energy eigenstates. These can be observed as oscillations in a balanced optical interferometer. We discuss the experimental feasibility of the method, and explore the possibility of discriminating between "pure" decoherence and that coinciding with energy transfer and heating.

I. INTRODUCTION

The Schrodinger cat is a well known example of the difficulty in clearly defining the border between the classical and quantum worlds. In this example, quantum theory allows for a macroscopic superposition of a dead and a live cat to exist while we have never been able to observe such a macroscopic superposition in nature. Indeed, this enigma has been the source of a century long debate.

To the best of our knowledge, only few attempts have been made so far to artificially create macroscopic superposition states. One attempt dealt with a superposition of two states of a multi-photon cavity field [1]. A second dealt with a superposition of a magnetic flux direction, formed by two macroscopic counter propagating electron currents [2]. Spatially separated superpositions of a trapped ion have been prepared and probed [3], and Bose Einstein condensates have also been examined [4]. Work on handedness of chiral molecules may also be considered relevant to this topic [5]. Microscopic, mechanical oscillators have been extensively discussed as well [6, 7], and experiments are now entering the regime where quantum effects become observable [8].

In this paper, we discuss a general oscillating massive object and its decoherence in the position basis, the basis which stands at the base of our classical perception. This spatial decoherence, also called "localization", is predicted by numerous models for environment-induced decoherence that are put forward to explain the appearance of classical reality from an underlying quantum world [9]: objects become localized in position due to their interaction with the environment. Of special interest is "pure" decoherence where localization can happen even without the transfer of energy, e.g., in a double-well potential. In order to reproduce the absence of macroscopic superpositions, most decoherence models use the mass of the decohering object as a central parameter along with parameters such as time and spatial splitting of the superposition. Indeed, recent seminal experiments on matter wave diffraction have tried for the first time to explore a

region of mass values beyond the usually experimentally feasible masses of elementary particles [10]. The visibility loss in the diffraction pattern is then a measurable signal of spatial decoherence.

Interference experiments with freely propagating objects, however, become increasingly hard to perform with larger masses for two main reasons: first, the de Broglie wavelength becomes smaller and the required diffraction gratings become more difficult to fabricate. Second, the spatial superposition created by diffraction is increasingly sensitive to decoherence because it is more difficult to isolate the freely propagating system from its environment. This renders a controlled experiment with large masses extremely difficult.

In this paper we propose a novel type of interference experiment in which no grating and no free propagation are needed. In fact, we avoid all together the need to create a well separated spatial superposition, and hence the way should be open to perform controlled decoherence experiments with large masses. Our experiment is based on an optical interferometer to probe the state of an oscillating mass, e.g. a nano bead or a mechanical oscillator. Contrary to previous work concerning oscillating mirrors [11], a symmetric ring interferometer is used, and the oscillator is not needed to have a high reactivity. We show that this setup can distinguish between different models of decoherence dynamics so that information about this subtle process can be obtained experimentally.

The next section describes the experimental setup. The theoretical model is presented in Sect. III, and solved approximately in Sect. IV. In Sect. V the experimental requirements are evaluated for specific examples. General conclusions are put in Sect. VI.

II. EXPERIMENTAL SETUP

The experimental setup we propose is sketched in Fig. 1: an object of mass m is confined in a potential $V(x)$ which can for all practical purposes be arranged in

such a way that only the motion along one direction is relevant, the x -axis, say. We assume in this paper a harmonic confinement, $V(x) = \frac{1}{2}m\omega^2x^2$. The object is held at the center of a ring interferometer, formed by massive mirrors (M) and an in-out coupling mirror (CM). The symmetry axis of the harmonic potential coincides with the plane of the beam splitter (BS), and hence with the symmetry axis of the whole setup. The BS and phase shifter (PS) prepare a symmetric photon mode, which excites a superposition (with zero phase shift) of right and left circulating travelling waves in the ring cavity. The BS and PS also act as a measurement apparatus for the outgoing modes, sending all anti-symmetric modes into the detector D . This is so because anti-symmetric modes of the cavity, are constructed from right and left circulating beams with a phase shift. These will be coupled out of the cavity through the CM in two separate directions. The PS will then reduce their phase difference to π as in a normal Mach-Zehnder apparatus, whereby the BS will then determine constructive interference in the direction of D .

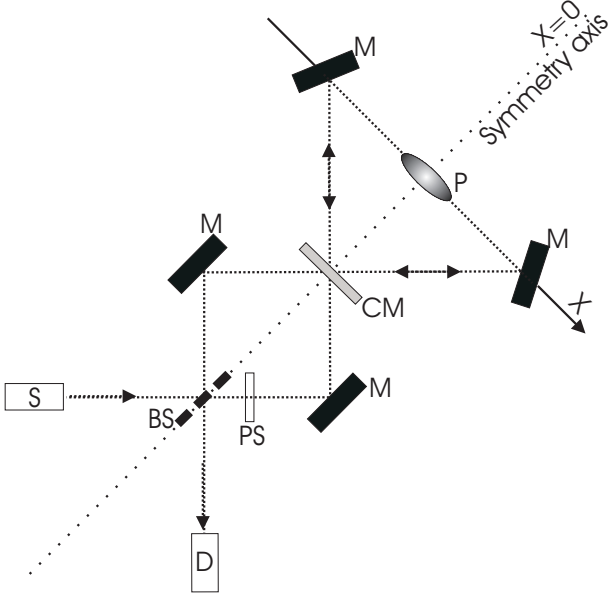


FIG. 1: Setup of the experiment. An atom or a more massive oscillating object, e.g. a nano bead or a two sided foil mirror is held in a harmonic potential (P). An incoming photon is split and "hits" the object from both sides. The source (S), the beam splitter (BS) and the phase shifter (PS) form a preparation system which ensures that the photon mode is symmetric with respect to the symmetry axis. (PS compensates the phase difference between the reflected and transmitted wave at the beam splitter.) The same system acts as a detection system whereby the anti-symmetric photon mode is sent to detector D . The potential is symmetric about the symmetry axis as well. If, for example, the object is initially prepared in a state of well-defined parity (e.g. the ground state of the potential), its final state will remain a parity eigenstate unless decoherence breaks the initial symmetry of the photon+object system.

The experimental procedure we have in mind is the following: at $t < 0$ the object is prepared in some equilibrium state at a given temperature. At $t = 0$ the preparation stops, and the environment, be it a thermal bath or some tailored environment, becomes dominant in the dynamics of the system. At $t = t_p$, a probe light pulse is sent into the ring interferometer and interacts with the object. The consequent measurement of the probe pulse which exits the interferometer after the interaction, determines if the even symmetry of the initial photon has been altered. In principle also the energy change of the outgoing photon may be measured, but in this paper we make no use of this option.

We note that the operation of the ring interferometer is not qualitatively affected when working with a "transparent" object like an atom or a thin mirror with high transmission. For ease of demonstration we will first describe a single atom. The potential could be provided in this case by a magnetic trap [12]. Following that, we will extend the treatment to a massive nanoparticle to show how the experimental sensitivity scales with mass and temperature.

To conclude, the scheme provides an experimental measure of decoherence which may be used for probing large mass objects. It is interesting to note that future technologies may enable confinement of massive objects also in potentials other than harmonic, in which case decoherence can lead to a clearer signature of spatial localization without energy transfer ("pure" decoherence). However, in this work, we show that already for the most feasible of large mass potentials (the harmonic well), the ring interferometer is able to distinguish between different decoherence scenarios, and hence we truly present a realizable scheme for the probing of decoherence with large masses.

III. MODEL

We use standard techniques of open system quantum dynamics to model the experiment sketched in the previous section. The initial state of the system (atom or nanoparticle) is described by a density matrix ρ_A , which represents thermal equilibrium in the harmonic trapping potential at temperature T_0 . Up to some probing time $t = t_p$, the system evolves according to a Liouville-von Neumann equation

$$\dot{\rho}_A = \frac{i}{\hbar} [H_S; \rho_A] + L[\rho_A]; \quad (1)$$

with the harmonic oscillator Hamiltonian

$$H_S = \frac{p^2}{2m} + \frac{m\omega^2}{2}x^2 \quad (2)$$

and a dissipative functional L that describes the influence of the environment on the system. Its expression is detailed below.

Around time t_p , a light pulse is injected into the cavity to probe the state of the oscillator. The pulse sent into the cavity has a center frequency close to a cavity resonance and a narrow bandwidth compared to the free spectral range (FSR). We assume that the oscillation frequency is much smaller than the FSR so that the interaction of the system with the field can only couple degenerate cavity modes. For simplicity, we neglect the light scattered by the object into higher transverse cavity modes. With a two-sided mirror foil as the object, this assumption becomes more realistic. The field in the cavity can then be described by only two degenerate modes with even and odd symmetry. As shown in Appendix A, the interaction Hamiltonian is given by

$$H_{int} = \hbar g (a_e^\dagger a_o + a_o^\dagger a_e) \cos(2kx) + a_e^\dagger a_o + a_o^\dagger a_e \sin(2kx) \quad (3)$$

where a_e and a_o are the boson operators for the even and odd cavity modes, respectively, $k = 2\pi/\lambda$ is the cavity wave number, and g is the coupling strength, which we estimate below. The excitation of the even mode is governed by the term

$$H_{pump} = \hbar \gamma_e^\dagger(t) \gamma_e(t) a_e; \quad (4)$$

where the pump amplitude is an operator whose state allows to describe any photon statistics of the incoming pulse. The leakage of photons out of the cavity is determined by the transmissivity of the coupling mirror (CM). This process is accounted for by the Liouville functional

$$L^{cav}[A_F] = 2 \sum_{i=e,o} \gamma_i A_F a_i^\dagger \frac{1}{2} [a_i^\dagger a_i; A_F]_+; \quad (5)$$

where γ_i is the finite cavity linewidth (HWHM), $[;]_+$ denotes the anti-commutator, and A_F is the joint density operator of the system and the cavity field modes. We assume for simplicity that all photons leaking out are actually detected with unit efficiency. Thus, the photon rate at the "odd" detector (D) is given by 2 times the number of odd photons in the cavity.

As a signal, we will consider the average photon number detected within the time interval $[t_p; t_f]$, given by

$$N_o = 2 \int_{t_p}^{t_f} \text{Tr} a_o^\dagger a_o A_F(t) dt; \quad (6)$$

The upper bound of the integration, t_f , is chosen such that the detected photon rate is negligibly small by this time. The pulse length, and hence the detection window, is kept short compared to the decoherence timescale of the system.

We focus in this paper on two different dissipative functionals that describe opposite extremes of dissipation and decoherence. The functional

$$L^{dec}[A] = \frac{D}{\hbar^2} [x; [x; A]] \quad (7)$$

describes pure spatial decoherence (D is the classical momentum diffusion coefficient), while

$$L^{therm}[A] = \frac{\hbar}{2} [b^\dagger b; A]_+ + \frac{\hbar}{2} [b^\dagger b; A]_+ \quad (8)$$

describes pure thermalization towards a temperature $k_B T_0 = \hbar \ln(\hbar/\hbar_0)$ [9, 13]. In the second case, we use creation and annihilation operators for the system oscillator.

Pure spatial decoherence can localize a system without the transfer of energy, for example in a deep double-well potential or through recoil-free scattering of probe particles. In quantum Brownian motion, this corresponds to the limit where the environment correlation time is so short that the rotating wave approximation with respect to the system's oscillation frequency cannot be made and terms like b^\dagger and b^2 are retained in the interaction with the environment [14]. These terms drive the system from the initial ground state $A(0) = |j\rangle\langle j|$ to a squeezed state. Therefore, after some time $t_p > 0$, its density matrix in energy basis will contain higher excited states such that off-diagonal elements become populated. Thermalization (8), on the other hand, simply redistributes the weights of the diagonal elements $\ln |j\rangle\langle j|$. The coherences of the energy eigenstates produce a breathing motion of the spatial density which can be detected by the probe pulse as t_p is varied. This signal then distinguishes spatial decoherence from thermalization, and allows us to probe pure decoherence for a massive body.

IV. ANALYTICAL SOLUTION

In this section, we work out the system density operator under the action of the decoherence models of the previous section, and analyze how it leaves a characteristic trace in the cavity modes operators.

A. Approximations

We summarize first the approximations we make to arrive at an analytical solution.

(i) The most significant difference of our approach compared to related work on mobile mirrors is the "sudden approximation": we assume that the duration of the pulse is short compared to the system oscillation period. Since the damping rate also determines the actual pulse length inside the cavity, we require

$$\text{min}(1/\gamma; \tau) \ll \tau \quad (9)$$

In this limit, the system's motion is "frozen" while the pulse is applied, and the Heisenberg equations for the photon mode operators can be solved without taking into account the dynamics of the system operators.

(ii) At the same time, the pulse must be sufficiently long in order to restrict the cavity dynamics to the two degenerate modes mentioned previously. This is valid when the inverse pulse length is small compared to the cavity free spectral range (FSR). Combining this with the "bad cavity limit" assumed below (1), but excluding a too small cavity resonance, we have

$$1 = \frac{\gamma}{\text{FSR}} < \text{FSR} : \quad (10)$$

(iii) Decoherence can be described by a dissipative functional as in Eq. (1) if the system is weakly coupled to its environment and decoherence is happening slowly on the timescale set by the oscillation period $2\pi/\omega$. This requires the inequality

$$\gamma_{th} \ll \omega \quad (11)$$

for the thermalization model (8). For the pure spatial decoherence model (7), we require that it takes more than one oscillation to increase the average system energy by one quantum $\hbar\omega$. This leads to

$$\gamma_{th} \ll \omega \quad (12)$$

where the rate

$$\frac{D}{\hbar m} \quad (13)$$

gives the depletion of the system ground state, see e.g. Föhlman et al. in [12]. Given Eq. (12), depletion happens slowly on the scale of the oscillation period. In both cases, the oscillator has a large quality factor.

B. Decoherence

We now show that the dissipative evolution can be integrated in terms of the system covariances in position and momentum. For the equilibrium initial state we consider here, the mean values $\langle x \rangle$, $\langle p \rangle$ vanish at all times by symmetry. Using the spatial decoherence functional (7), we get from the Liouville-von Neumann equation (1)

$$\frac{d}{dt} \langle x^2 \rangle = \frac{1}{m} \langle \dot{x}^2 \rangle = \frac{1}{m} \langle p^2 \rangle \quad (14a)$$

$$\frac{d}{dt} \langle p^2 \rangle = -\frac{1}{m} \langle \dot{p}^2 \rangle = -\frac{1}{m} \langle \ddot{x}^2 \rangle = -\frac{1}{m} \langle -m\omega^2 x^2 \rangle = \omega^2 \langle x^2 \rangle \quad (14b)$$

$$\frac{d}{dt} \langle xp + px \rangle = \frac{1}{m} \langle \dot{x}\dot{p} + \dot{p}\dot{x} \rangle = \frac{1}{m} \langle \ddot{x}x + x\ddot{x} \rangle = \frac{1}{m} \langle -m\omega^2 x^2 \rangle = -\omega^2 \langle x^2 \rangle \quad (14c)$$

Characteristic for spatial decoherence is that only the momentum width is increased by the diffusion coefficient D . This "squeezes" the system state in the phase plane, while the dynamics in the harmonic potential subsequently leads to a rotation. The coupled equations (14a-c) can be solved, with the result (see, e.g., [14])

$$\langle x^2 \rangle_t = \langle x^2 \rangle_0 + \frac{\hbar}{2m} (2\gamma_{th} t - \sin 2\gamma_{th} t) \quad (15a)$$

$$\langle p^2 \rangle_t = \langle p^2 \rangle_0 + \frac{\hbar m}{2} (2\gamma_{th} t + \sin 2\gamma_{th} t) \quad (15b)$$

$$\langle xp + px \rangle_t = \frac{\hbar}{2} (1 - \cos 2\gamma_{th} t); \quad (15c)$$

where the decoherence rate γ_{th} has been defined in (13). We have used that equipartition holds in the initial state, $\langle p^2 \rangle_0 = m \langle \dot{x}^2 \rangle_0$, which is obviously true for an initial thermal state. Note that the decoherence Liouvillean does not describe a stationary solution in the limit $t \rightarrow \infty$, this is because we neglected friction.

For the thermalization model (8), the variances can be computed similarly, and we find

$$\langle x^2 \rangle_t = \langle x^2 \rangle_0 + \frac{E(T_0)}{m} (1 - e^{-2\gamma_{th} t}) \quad (16a)$$

$$\langle p^2 \rangle_t = \langle p^2 \rangle_0 + E(T_0)m (1 - e^{-2\gamma_{th} t}) \quad (16b)$$

$$\langle xp + px \rangle_t = 0 \quad (16c)$$

$$\gamma_{th} = \frac{\hbar}{2} \frac{\omega^2}{\omega_0}; \quad (16d)$$

where $E(T_0) = \frac{1}{2} \hbar \coth(\hbar \omega / 2k_B T_0)$ is the average oscillator energy at equilibrium with the environment (temperature T), and where the rate γ_{th} characterizes both the approach towards thermal equilibrium and the damping of the system's average position and momentum.

The key benefit of this formulation in terms of covariances is that it provides an exact solution for the system density operator [15, 16]. The reasons for this are the thermal initial state we consider here and the Liouville functionals (7, 8) that are bilinear in $x; p$. We shall work with the Wigner representation $W(x; p; t)$ of the density operator that has properties similar to a classical phase space distribution [17]. For example, expectation values of symmetrized system operators $S(\hat{x}; \hat{p})$ are computed according to

$$\langle S(\hat{x}; \hat{p}) \rangle_t = \int \frac{dx dp}{2\pi\hbar} S(x; p) W(x; p; t); \quad (17)$$

Given the covariances, we find the Wigner function

$$W(x; p; t) = N(t) \exp[-G(x; p; t)] \quad (18a)$$

$$2G(x; p; t) = \frac{x^2}{\langle x^2 \rangle_t} + \frac{1}{\langle p^2 \rangle_t} p^2 - \frac{C_t x}{A_t} \quad (18b)$$

$$\frac{C_t}{A_t} = \frac{\langle xp + px \rangle_t}{2\langle x^2 \rangle_t} \quad (18c)$$

$$\frac{1}{N(t)^2} = \frac{\langle x^2 \rangle_t \langle p^2 \rangle_t - \frac{1}{4} \langle xp + px \rangle_t^2}{\hbar^2}; \quad (18d)$$

Note that for the normalization factor, one finds $N(t) = 1/2$ because of the uncertainty relations.

C. Short probe pulse

In a frame rotating at the cavity resonance frequency, the Heisenberg equations for the photon operators are

$$\dot{a}_e = -i\gamma (\cos(2kx) a_e + \sin(2kx) a_o) - a_e + i(t) + e \quad (19a)$$

$$\dot{a}_o = -i\gamma (\cos(2kx) a_o - \sin(2kx) a_e) - a_o + i(t) + o \quad (19b)$$

where e_{j0} are quantum noise operators that can be neglected as long as we calculate normally ordered quantities, such as the intensity. In the sudden approximation, we assume that the system position operator x does not change during the pulse duration. It can then be treated as a constant that commutes with the photon operators.

The initial condition just before time t_p is vacuum for both cavity modes. The evolution of the odd mode is then given by (neglecting terms with vanishing expectation value)

$$a_o(t_p + t) = i \sin(2kx) \frac{g e^{t \cos g t} e^{-t \sin g t}}{g^2 + \omega^2} \quad (20)$$

for $0 < t < \tau$, where τ is the pulse length, and the pulse shape was taken as a mesa-function: $a_o(t) = 1$ for $0 < t < \tau$, otherwise it vanishes. With this choice, $a_o(t) = (2\pi)^{-1} a_{in}$, where a_{in} is the boson operator of the probe pulse incident on the cavity.

The average number of odd photons N_o at the detector during the time window $[t_p, t_f]$ can be calculated by integrating $2 a_o^\dagger(t) a_o(t)$, see Eq. (6). As mentioned in Sec. IV A, we consider here the bad cavity limit where

1. In this limit, we may set $t_f = t_p + \tau$, and the integration yields the simple result

$$N_o = R \hbar a_{in}^\dagger a_{in} \sin^2(2kx) i \quad (21)$$

with

$$R = \frac{g^2}{(g^2 + \omega^2)^2} : \quad (22)$$

The average over the field and system operators in Eq. (21) can be computed independently because we have assumed that the system + field density operator factorizes at $t = t_p$. The signal is thus proportional to the mean photon number of the probe pulse, $\hbar a_{in}^\dagger a_{in} i = N_{in}$. We discuss the signal fluctuations in Sec. IV D below. For the average over the system, the Wigner function (18b) gives after one elementary integration

$$\begin{aligned} \hbar \sin^2(2kx) i_{t_p} &= \frac{1}{2\pi} \int dx dp \sin^2(2kx) W(x; p; t_p) \\ &= \frac{1}{2} \exp(-8k^2 \hbar x^2 i_{t_p}) ; \end{aligned} \quad (23)$$

where the variance $\hbar x^2 i_{t_p}$ has been calculated in Eqs. (15a) and (16a).

We observe that the solution (20) illustrates how our detection scheme conserves parity. Consider an incident pulse in a single photon state, $j(t_p) i = a_{in}^\dagger j i$, and assume that the odd detector clicks. This updates the system state to

$$|\text{odd click}\rangle = \frac{1}{\sqrt{2}} K \sin(2kx) |-\rangle \sin(2kx) ; \quad (24)$$

where K is the normalization. If the system has been in a state $|+\rangle$ with definite parity, this state has the opposite

one. Similarly, a click in the even mode detector updates the system state to a state with the same parity. In both cases, the "collapse" of the wave function does not lead to an asymmetric state with less well defined parity. This ensures that symmetry of the system state can only be changed by decoherence.

The factor R in Eq. (22) gives basically the probability that an incident photon actually interacts with the system. This can be seen from the number of even photons that is given by

$$N_e = R N_{in} + R N_{in} \cos^2(2kx) i \quad (25)$$

where $R = \frac{4}{(g^2 + \omega^2)^2}$. The first term is independent of the system position and gives the photons that did not interact with the system. This number reduces to N_{in} for a vanishing coupling, $g \rightarrow 0$. The second term has a similar structure as Eq. (21), only the system operator with even parity occurs. It adds up with N_o to $R N_{in}$, similar to the two output ports of an interferometer. The fraction of useful photons is thus $R = (R + R) = \frac{4}{g^2 + \omega^2}$.

For typical experimental conditions that we discuss in Sec. V A, the probe wavelength is large compared to the width of the system position distribution ("Lamb-Dicke limit"). We can then expand the exponential in Eq. (23) to get

$$N_o = 4R N_{in} k^2 \hbar x^2 i_{t_p} ; \quad (26)$$

so that a larger signal is obtained with a shorter probe wavelength. This scaling breaks down, however, in the extreme case of λ being comparable or shorter than the position width ("anti-Lamb-Dicke limit"). This may also occur in the long-time limit, after heating has significantly broadened the position distribution. The signal then no longer increases linearly with $\hbar x^2 i_{t_p}$. The exponential in Eq. (23) vanishes, and the signal saturates at $N_o = R N_{in} = 2$ regardless of the value of the $\hbar x^2 i_{t_p}$. In this limit, the probe pulse is no longer able to extract information about the system.

We note that the same result $N_o = R N_{in} = 2$ may be arrived at on much shorter time scales (even for $t_p = 0$) when the initially prepared system is already in the anti-Lamb-Dicke limit. The system then heats as a result of photon scattering ("back action"). The exponential $\exp(-8k^2 \hbar x^2 i_0)$ in Eq. (23) is in fact the Debye-Waller factor for this scattering process. It gives the probability of the system still occupying the ground state after the photon pulse has impinged on it. In the anti-Lamb-Dicke limit, the Debye-Waller factor is zero, and the system makes with probability unity a transition to a vibrationally excited state. Since the detection of an odd photon is directly correlated, due to symmetry conservation, to a transition from the even ground state to an odd state, it occurs for one half of all useful photons $R N_{in}$ that actually interacted with the system.

One may also understand this result in the position basis. In the anti-Lamb-Dicke regime, the system position

is smeared out over many probe wavelengths so that the phase of the backscattered light varies randomly from 0 to 2π . On average, one half of those photons that interact with the system are sent into the odd detector.

D. Signal fluctuations

For the discussion of the signal to noise ratio in Sec. VB, we also need the fluctuations of the odd detector signal (21).

The variance N_o^2 can be computed from the factorized state $\rho_{AF}(t_p)$ as well. For a probe pulse in a coherent state, we find

$$N_o^2 = R^2 N_{in} (N_{in} + 1) h \sin^4(2kx) i_{tp}^2$$

$$N_{in}^2 h \sin^2(2kx) i_{tp}^2 \quad (27)$$

and

$$h \sin^4(2kx) i_{tp}^2 = \frac{1}{8} [3 - 4e^{-8k^2 \hbar x^2 i_{tp}} + e^{-32k^2 \hbar x^2 i_{tp}}]$$

$$3(4k^2 \hbar x^2 i_{tp})^2 : \quad (28)$$

In the last step, we made the long-wavelength expansion as in Eq. (26).

If the system were located at a fixed position, the terms proportional to N_{in}^2 in Eq. (27) would cancel, leading to number fluctuations limited by shot noise. This is not the case here, however, because of the finite position uncertainty. For the Gaussian distribution at hand, the fluctuations of x^2 are of the same order and even somewhat larger than their mean value $\hbar x^2 i$ itself. In the long-wavelength limit, Eq. (27) becomes

$$N_o^2 = R^2 (4k^2 \hbar x^2 i_{tp})^2 2N_{in}^2 + 3N_{in} : \quad (29)$$

For completeness, we also give the opposite limit of a short wavelength, although it is experimentally more challenging. Recall that the average signal $N_o = RN_{in} = 2$ arises because the phase $\phi = 2kx$ is uniformly distributed between 0 and 2π , and the fraction of photons in the odd detector proportional to $h \sin^2 \phi = \frac{1}{2}$. The variance then becomes $N_o^2 = R^2 (\frac{1}{8} N_{in}^2 + \frac{3}{8} N_{in})$, where the second term is due to shot noise and the first is due to the variance $h \sin^4 \phi = h \sin^2 \phi^2 = \frac{1}{8}$. This estimate agrees with the anti-Lamb-Dicke limit of the general Eq. (27).

V. DISCUSSION

We show in this section that experimental conditions should exist where it is possible to spot the difference between spatial decoherence and thermalization by measuring the photon signals outside the cavity.

vibration frequency ω	50 kHz
pulse length	20 ns
cavity line width ω_c	50 MHz
free spectral range FSR	1 GHz
wavelength	785 nm
Lamb-Dicke parameter $(k x_0)^2$	0.075
coupling strength g	10 kHz
decoherence rate γ	1 kHz

TABLE I: Realistic experimental parameters for a Rb atom fulfilling the validity conditions of the calculation, and yielding a signal to noise ratio larger than 3 in a spectral analysis (as discussed around Eq.(34)).

A. Example I: Single atom

The system we consider in the first example is a single rubidium atom trapped in a tightly confining magnetic trap. The chosen parameters are listed in Table I. The oscillation frequency is similar to those achieved with magnetic traps on atom chips [12]. For such trapping frequencies, ground state cooling leads to a spatial width $\hbar x_0^2 = \frac{1}{2m\omega}$ of the order of $\lambda_D = (2m\omega)^{-1/2} = 34$ nm. Trapped ions cooled to the ground state with sideband cooling are also a good system for this purpose. We note that a cold thermal state would be sufficient as well. For the sake of this example, we choose a relatively long wavelength close to the D1 rubidium line. This gives a resonantly enhanced AC polarizability, while absorption and spontaneous emission can still be minimized with a detuning of several linewidths. The corresponding coupling strength g is estimated in the Appendix. Pulse length, cavity linewidth and free spectral range are chosen to comply with the approximations defined by Eqs. (9) and (10).

The last quantity, the decoherence rate γ , depends on the specifics of the system. For an atom in a miniaturized electromagnetic trap on an atom chip, estimates for heating due to magnetic field fluctuations are in the range of 1 s^{-1} [12]. Other environmental perturbations can be added at will to enhance this rate in a controlled way. In fact, a tunable decoherence source is suitable for the unambiguous, experimental discrimination between decoherence and thermalization-induced dynamics.

The signal in the odd photon detector given by Eqs. (21) and (23) is plotted in Figure 2, using the spatial decoherence model (7) and the parameters given in Table I. The signal shows an overall increase because the environment heats the system and broadens its position distribution. The important feature of this plot are the superimposed oscillations. They stem from the breathing motion of the wave packet and are a telltale sign of spatial decoherence that affects position and momentum in a non-equivalent manner. Indeed, Eq. (14b) shows that decoherence only increases the momentum width which leads to a squeezed phase space distribution. The dy-

namics in the harmonic potential makes this elongated distribution rotate at the frequency ω so that its projection onto the position or momentum axis oscillates in width at an angular frequency 2ω (as expected from Eqs. 14).

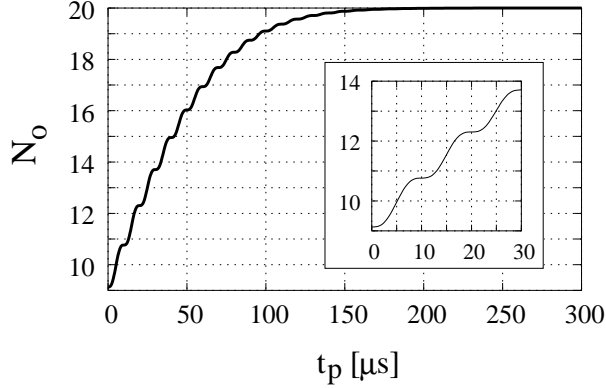


FIG. 2: Average photon number $N_o(t_p)$ hitting the odd detector (D) for $N_{in} = 10^9$ incoming photons, as a function of the delay time t_p in microsecond at which the measurement takes place. In the inset the initial oscillations are magnified. Parameters are given in Table I (Rb atom).

B. Signal visibility

Next we here discuss ways to extract the oscillations at 2ω of the odd detector signal that are characteristic for spatial decoherence.

Let us consider probing times t_p in the range where the system is in the Lamb-Dicke limit. That is, in Fig. 2, we are well before the saturated regime, $t_p < 100$ s. The number of odd photons is then given by Eq. (26) which, combined with Eq. (15a) yields the peak-to-peak amplitude of the breathing oscillations

$$N_{osc} = 8N_{in}R(k_0)^2; \quad (30)$$

where $(k_0)^2 = \hbar k^2 = 2m$ is the so-called Lamb-Dicke parameter. It is interesting to note that the oscillation amplitude (30) depends neither on the initial system state nor on the delay time t_p for the probe pulse [18]. However, the last three factors, R , k_0 , and ω are all less than unity, and a significant photon number can only be obtained with a bright probe pulse, $N_{in} \gg 1$. In the example given above, $N_{in} = 10^9$ for a 20 ns pulse (10^{10} J per pulse), and this large number compensates for the small fraction of 'useful photons' $R \approx 10^{-8}$. The signal can be improved a lot with a larger coupling strength g . For the optimal value $g = \sqrt{2}$, the ratio R takes its maximum value $1/4$. The signal amplitude can also be increased with a shorter probe wavelength as long as one remains in the Lamb-Dicke limit.

The contrast C_{osc} of the breathing oscillations is defined by dividing the oscillation amplitude (30) to the smoothed background signal. Since that background increases with t_p (in the Lamb-Dicke regime), the contrast is time-dependent. In terms of the initial system temperature T_0 ,

$$C_{osc}(t_p) = \frac{2}{\coth(\hbar = 2k_B T_0) + t_p}; \quad (31)$$

where the dependences on photon number, detection probability and probe wavelength have cancelled. The initial contrast is maximized for low temperatures $k_B T_0 \ll \hbar$ when the system is cooled close to the ground state. Even then it is limited by the small ratio $\omega = \hbar / (2m\lambda^2)$, see Eq. (12). For higher temperatures, the contrast decreases like $\hbar = k_B T_0 \ll 1$. The contrast reduction with increasing t_p happens on the time scale $\coth(\hbar = 2k_B T_0) = \hbar / (2m\lambda^2)$, where decoherence has approximately doubled the position variance compared to its initial value. This time scale is of order $1/\omega$ if the initial temperature is low. Otherwise, when the initial position distribution is already quite broad, it is of order $k_B T_0 = (\hbar / (2m\lambda^2))$, so the decoherence needs longer to double the initial width.

To get a realistic estimate for the visibility of the oscillations, however, one has to take into account the fluctuations of the detector signal. The variance N_o^2 is given in Eq. (29) for the Lamb-Dicke limit. It shows a super-Poissonian scaling with N_{in}^2 to leading order so that we get a signal to noise ratio

$$S/N(t_p) = \frac{N_{osc}}{N_o} = \frac{C_{osc}(t_p)}{(2 + 3N_{in})^{1/2}}; \quad (32)$$

which is much smaller than unity. In order to resolve the oscillations, the S/N ratio has to be enhanced by repeating the experiment a number of times

$$n_{ex} = 10 = [S/N(t_p)]^2; \quad (33)$$

which ensures that the measured oscillation amplitude at an antinode exceeds the background noise level by three standard deviations. For short enough times this condition yields a number of $n_{ex} = 10$ recordings for a given time t_p .

Alternatively, the oscillations can be extracted from the signal frequency spectrum in terms of the peak they give at 2ω . If we assume that the increase of the background is negligible on the time scale 2ω , the signal fluctuations give an approximately white noise. In terms of the weight of the peak at 2ω , we find an improvement by a factor $(T = t)^{1/2}$ with respect to the signal to noise ratio (32), where T is the maximum probing time in the data set and t the time resolution. This shows that the sudden approximation (a small value of ω) is actually required to extract the signal. We can take into account the slow increase of the background in an approximate way by writing the spectral signal to noise ratio as

$$S/N(2\omega) = \frac{(T = t)^{1/2} S/N(t_p = T/2)}{(2 + 3N_{in})^{1/2} \coth(\hbar = 2k_B T_0) + T/2}; \quad (34)$$

The signal to noise ratio shows a maximum for a specific observation time

$$T_{\text{opt}} = \frac{\coth(h = 2k_B T_0)}{2} \quad (35)$$

which is $T_{\text{opt}} \rightarrow 1$ for low initial temperatures. It is interesting that the system should be monitored up to the time where the contrast (31) of the oscillations decreases. As a characteristics of the efficiency of the detection process, we obtain the maximum S/N

$$\max S/N(2) = \frac{\tanh(h = 2k_B T_0)}{2}^{1/2} : \quad (36)$$

The spectral signal to noise ratio can be significant, i.e. we get $\max S/N(2) > 3$ for the system parameters of Table I, and it thus provides an evidence for the oscillations. Note, however, that this signal is obtained from the records for the whole time series from 0 to T_{opt} . That is, a measurement repetition $n_{\text{ex}} = T_{\text{opt}} = 1$ is necessary. On taking into account that a time resolution $\Delta t = 0.1$ is required for getting such a significant S/N, we arrive at a necessary number of measurements $n_{\text{ex}} = 10$. This condition is similar to the one we obtained for the resolution of the oscillations at a single point t_p . This result also justifies the use of a controlled decoherence source to enhance the decoherence rate. For example, with the parameters given in Table I, about 10^4 measurements are required for evolutions in the range of 0 to 100 s to get the signal to noise ratio larger than 3.

C. Example II: Nanoparticle

Finally, we come back to the main motivation of this work and consider the decoherence of massive systems. As examples of such a nanoparticle we think of recently realized nano electromechanical oscillators (NEMOs) [19] or beads, which may be put in an harmonic confining potential by holding their edges or by suspending them in a fluid by electric (e.g. Paul trap), magnetic, or optical interaction (optical tweezers for small beads).

The crucial parameter is the initial temperature which makes a difference with respect to the case of single atoms. While atoms can be routinely cooled down to the ground state of oscillation in a trap by various optical methods, there is no such efficient cooling scheme for arbitrary massive objects. We can safely assume that nanoparticles can be cooled down to below 1K or even, in the near future, to the mK range (e.g. using optomechanical feedback [11] or special cryogenics). With experimentally feasible trapping frequencies in the range of MHz, such temperatures are still large, $h \gg k_B T_0$, and the initial vibrational state of the system is highly excited.

On the other hand, for large enough masses, such a temperature range is sufficiently low to reach the Lamb-

mass m	$< 10^{-15}$ kg
vibration frequency ω	2 MHz
pulse length	30 ns
decoherence rate γ	100 kHz
initial temperature T_0	1 mK
max S/N	0.1
T_{opt}	100 s
n_{ex}	10^6

TABLE II: First block: parameters for a reference nanoparticle fulfilling the validity conditions of the calculation. Second block: calculated maximum of the 'signal to noise' ratio of the spectral analysis and the maximum recorded evolution time. Third block: the estimated number of experimental runs in order to achieve three standard deviations and the verification of the decoherence signal.

Dicke regime,

$$k^2 \hbar x^2 i_0 = (k_0)^2 \frac{2k_B T_0}{h} \gg 1; \quad (37)$$

where $(k_0)^2 = \hbar k^2 = 2m$ is again the Lamb-Dicke parameter (see Eq.(30)). According to Eq. (23), this is the basic necessary condition for the proposed detection scheme to work. We can then use the general result of Eq. (36) and expand the tanh function to lowest order:

$$\max S/N(2) = \frac{h}{2k_B T_0}^{1/2}; \quad (38)$$

and similarly from Eq. (35):

$$T_{\text{opt}} = \frac{2k_B T_0}{h} : \quad (39)$$

The requirements for the experiment can be quantitatively estimated on the basis of these equations, regardless of the specific implementation of the scheme.

One important quantity is the number of measurements needed to get a statistically significant signal of the oscillations in the odd photon detector. First, a number of $T_{\text{opt}} = 100$ measurements has to be carried out to monitor the decoherence evolution from $t_p = 0$ to $t_p = T_{\text{opt}}$. Second, this full evolution has to be recorded a number of about $10 = (\max S/N)^2$ times to reach, by spectral analysis, three standard deviation from the noise level. The total number of measurements is then

$$n_{\text{ex}} = 10 (\max S/N)^2 = 10 (2k_B T_0/h)^2; \quad (40)$$

which heavily depends on the initial temperature. It follows that the decoherence rate should be artificially enhanced to the maximum level allowed by the condition (11), i.e. $\gamma = 0.1$.

Estimates for a reference nanoparticle are assembled in Table II. For a trapping frequency $\omega = 2$ MHz, the decoherence rate can be as large as $\gamma = 2$ 100 kHz. In order to maximize the signal to noise ratio,

the pulse length can be as short as $\tau = 10$. For a cavity linewidth $\gamma = 2.50$ MHz, as the one in the Rb atom example, an initial temperature $T_0 = 1$ mK yields the ratio $\max S/N \approx 0.1$, and we get a number $n_{\text{ex}} \approx 10^6$ where one measurement takes a time about $T_{\text{opt}} = 2 \times 100$ s (not including the preparation time).

In many possible physical realizations, the coupling to the nanoparticle are independent of its mass, i.e. so are the spring constant of the trap, $K = m^{-2}$, and the parameter D of the decoherence functional (7). It is very interesting that $\gamma = D = K$ and, hence, the maximum signal to noise ratio in Eq. (38) is independent of the mass of the particle. This proves that the scheme can be extended to monitor the decoherence of massive particles. The mass, in fact, can be scaled up to a limit m_{cr} without degrading the signal. This limit is related to our assumption that the particle remains smaller than the wavelength so that it couples to the light field via its polarizability. The upper mass limit is $m_{\text{cr}} \approx 10^{15}$ kg, i.e. about 10^{10} Rb atoms, for a typical material density and visible light. The optimum time period to reach the maximum spectral visibility, on the other hand, depends on the mass $T_{\text{opt}} \propto m^{2/3}$, $T_0 = D$ and makes the necessary conditions of observing decoherence less demanding for smaller masses.

VI. CONCLUSION

To conclude, we have addressed the problem of observing the decoherence process in massive objects. Experimentally quantifying the process for large masses and different environments is of paramount importance for the accurate theoretical modeling of this subtle transition from quantum to classical.

Specifically, we have shown that it should be possible to study the decoherence of systems that are trapped. In contrast to conventional spatial dephasing experiments, in which the observed object is freely propagating, the presented scheme will allow for more isolation, and hence for a better control over the coupling to the environment. This is made possible by making use of a photon probe that scans the object for changes in its wave function. Furthermore, the suggested experimental scheme, bypasses the need to create a clearly separated spatial superposition. This need presents an ever growing technical difficulty for large masses in terms of the actual preparation procedure and in terms of the rate of decoherence. A "pure" decoherence signal is apparent even when no superposition was created initially. The only requirement in the present scheme is to prepare the system in an equilibrium state of an harmonic potential.

These features will greatly enhance the feasibility of a decoherence experiment with a scalable object mass. In addition, the interaction with optical cavity modes can be used to tailor the object's environment and to induce "decoherence on demand" [20].

In this paper, we have limited ourselves to objects

smaller than the wavelength that weakly scatter light. Future work will address moving mirrors that lead to a stronger optical signal. Preliminary results show that a similar Hamiltonian accounts for the coupling to the cavity modes so that most of the present analysis can be carried over, but with more favorable parameters.

Finally, we have focused on environmental decoherence. However, if the system may be isolated well enough so that the coupling to the environment does not mask other weaker processes of localization, then one may perhaps be able to study also other proposed models [21, 22].

Acknowledgments

C.H. and M.N. thank J. Eisert (Potsdam) for stimulating discussions. P.D. acknowledges the support by the National Scientific Fund of Hungary (Contracts No. T 043079 and T 034484) and that of the Bolyai Fellowship Programme of the Hungarian Academy of Sciences. R.F. would like to thank for their support the German Federal Ministry of Education and Research (BMBF), the Israel Science Foundation, and the European Union Research Training Network (MRTN-CT-2003-505032).

APPENDIX A: INTERACTION HAMILTONIAN

We describe the interaction between the electromagnetic field and the object by $\frac{1}{2} \epsilon E^2$, where ϵ is the polarizability and E the (linearly polarized) electric field. In second quantization, keeping only the even and odd cavity modes, the field can be written

$$E = \frac{\hbar \omega_c}{\epsilon_0 V} f a_e \cos(kx) + a_o \sin(kx) + \text{h.c.}; \quad (\text{A1})$$

where ω_c is the (common) mode frequency, the wavenumber $k = \omega_c/c$, V is the cavity mode volume. In the rotating wave approximation and adopting normal order, we hence find for the interaction

$$H_{\text{int}} = \frac{\hbar \omega_c}{2 \epsilon_0 V} a_e^\dagger a_e + a_o^\dagger a_o + a_e^\dagger a_e - a_o^\dagger a_o \cos(2kx) + a_e^\dagger a_o + a_o^\dagger a_e \sin(2kx); \quad (\text{A2})$$

We see here that the scattering from even into odd modes is accompanied by an anti-symmetric excitation of the object. If the photon leaves the cavity in the same mode, however, the object state is changed by the symmetric function $\cos(2kx)$. For the interaction Hamiltonian used in the main text, we have left out the part $a_e^\dagger a_e + a_o^\dagger a_o$ involving the total photon number. Since this is a conserved quantity, it only contributes a global phase factor to the system + field wave function.

Writing g for the prefactor in Eq. (A2), we get the coupling constant g . With an atom as system, we adopt

a two-level model for the AC polarizability and cast the coupling in the form

$$g = \frac{3}{8} \frac{\epsilon_c}{\epsilon_A} \text{FSR} \frac{A}{\epsilon_A} \frac{1}{\epsilon_c} \frac{A}{\epsilon_A} \quad (\text{A } 3)$$

where ϵ_A is the atomic resonance frequency and $1/\epsilon_A$ the corresponding radiative lifetime. A is the cross section of the cavity modes and $\text{FSR} = c/L$ the free spectral range. Eq. (A 3) assumes an excitation not too far off resonance, $|\epsilon_A - \epsilon_c| \ll \epsilon_A$. Typical parameters are $\text{FSR} = 10^8 \text{ s}^{-1}$, $A = 10^3$, $\epsilon_A = 10$, and give $g = 10^4 \text{ s}^{-1}$. This can be increased further with tighter focussing, smaller cavity lengths and working closer to resonance. A far off-resonant excitation with a shorter wavelength would improve the resolution of the position measurement. This is likely to be over-compensated by the smaller polarizability, since for ϵ well above a resonance transition, $1/\epsilon \approx 0$.

If the system is a nanoparticle with size smaller than

the wavelength, the polarizability can be written in the Clausius-Mossotti form

$$\epsilon(\omega) = 4\pi n_0^2 a^3 \frac{\epsilon(\omega)}{\epsilon(\omega) + 2}; \quad (\text{A } 4)$$

where $\epsilon(\omega)$ is the particle's permittivity. The factor $4\pi n_0^2 a^3 / (\epsilon(\omega) + 2)$ shows a resonance for example in metallic particles (collective plasma oscillation). A value ≈ 5 seems realistic while avoiding too large absorption losses. This gives a coupling

$$g = (2\pi)^2 \text{FSR} \frac{m}{A m_{\text{cr}}}; \quad (\text{A } 5)$$

where the 'critical mass' is defined in terms of the mass density ρ as $m_{\text{cr}} = \rho^3$. Typical numbers ($\rho = 1 \text{ g/cm}^3$, $m = 1 \text{ m}$) give $m_{\text{cr}} = 10^{15} \text{ kg}$. With the same numbers for the cavity mode as before, we get the fairly large value $g = \text{FSR} (m = m_{\text{cr}})$.

-
- [1] M. Bunn et al., Phys. Rev. Lett. 77, 4887 (1996).
 [2] C. H. van der Wal et al., Science 290, 773 (2000); J. R. Friedman et al., Nature 406, 43 (2000).
 [3] C. Monroe, D. M. Meekhof, B. E. King, and D. J. Wineland, Science 272, 1131 (1996).
 [4] J. Ruostekoski et al., Phys. Rev. A 57, 511 (1998).
 [5] Z. Vager, Chem. Phys. Lett. 273, 407 (1997) and references therein.
 [6] R. Folman et al., Eur. Phys. J. D 13, 93 (2001).
 [7] S. Bose et al., Phys. Rev. A 56, 4175 (1997); Phys. Rev. A 59, 3204 (1999); S. Mancini et al., Phys. Rev. Lett. 88, 120401 (2002); W. Marshall et al., Phys. Rev. Lett. 91, 130401 (2003).
 [8] I. Tutton et al., Phys. Rev. A 59, 1038 (1999); A. D. Armour et al., Phys. Rev. Lett. 88, 148301 (2002); I. Bargatin and M. L. Roukes, Phys. Rev. Lett. 91, 138302 (2003); X. M. H. Huang et al., Nature 421, 496 (2003); R. G. Knobel and A. N. Cleland, Nature 424, 291 (2003).
 [9] D. Giulini et al., Decoherence and the appearance of a classical world in quantum theory, Springer (1996), and references therein.
 [10] M. Amdt et al., Nature 401, 680 (1999); W. Schoellkopf and J. P. Toennies, Science 266, 1345 (1994); B. Brezger et al., Phys. Rev. Lett. 88, 100404 (2002).
 [11] V. Giovannetti and D. Vitali, Phys. Rev. A 63, 023812 (2001); P. F. Cohadon, A. Heidmann, and M. Pinard, Phys. Rev. Lett. 83, 3174 (1999); K. Jacobs, I. Tutton, H. M. Wiseman, and S. Schiller, Phys. Rev. A 60, 538 (1999).
 [12] J. Reichel, Appl. Phys. B 74, 469 (2002); R. Folman et al., Adv. At. Mol. Opt. Phys. 48, 263 (2002), B. Bederson, editor.
 [13] R. Alicki and K. Lendi, Quantum Dynamical Semigroups and Applications, Lecture Notes in Physics 286, Springer, Berlin (1987).
 [14] D. Kohen, C. C. Marston, and D. Tannor, J. Chem. Phys. 107, 5236 (1997).
 [15] F. Haake and R. Reibold, Phys. Rev. A 32, 2462 (1985).
 [16] G. W. Ford and R. F. O'Connell, Phys. Rev. D 64, 105020 (2001); J. Eisert and M. B. Plenio, Phys. Rev. Lett. 89, 137902 (2002).
 [17] N. G. van Kampen, Stochastic Processes in Physics and Chemistry, revised ed. (Elsevier, Amsterdam, 1992).
 [18] We expect, however, the oscillations to be damped at times where friction, that has been neglected in the pure decoherence functional (7), sets in.
 [19] X. M. H. Huang, C. A. Zorman, M. Mehregany, M. L. Roukes, Nature 421, 496 (2003).
 [20] P. A. Maia Neto and D. A. R. Dalvit, Phys. Rev. A 62, 042103 (2000).
 [21] G. C. Ghirardi, A. Rimini and T. Weber, Phys. Rev. D 34, 470 (1986); L. Diosi, Phys. Rev. A 40, 1165 (1989); G. C. Ghirardi, P. Pearle and A. Rimini, Phys. Rev. A 42, 78 (1990); I. C. Percival, Proc. R. Soc. London A 447, 189 (1994); P. Pearle and E. Squires, Phys. Rev. Lett. 73, 1 (1994); D. J. Fivel, Phys. Rev. A 56, 146 (1997).
 [22] R. Penrose, in Mathematical Physics 2000, edited by A. Fokas et al., Imperial College, London (2000)